Mechanism of Interannual to Decadal Variability of the North Atlantic Circulation

CARSTEN EDEN AND JÜRGEN WILLEBRAND

Institut für Meereskunde, Kiel, Germany

(Manuscript received 17 May 2000, in final form 25 September 2000)

ABSTRACT

A model of the Atlantic Ocean was forced with decadal-scale time series of surface fluxes taken from the National Centers for Environmental Prediction–National Center for Atmospheric Research reanalysis. The bulk of the variability of the oceanic circulation is found to be related to the North Atlantic oscillation (NAO). Both realistic experiments and idealized sensitivity studies with the model show a fast (intraseasonal timescale) barotropic response and a delayed (timescale about 6–8 yr) baroclinic oceanic response to the NAO. The fast response to a high NAO constitutes a barotropic anticyclonic circulation anomaly near the subpolar front with a substantial decrease of the northward heat transport and an increase of northward heat transport in the subtropics due to changes in Ekman transport. The delayed response is an increase in subpolar heat transport due to enhanced meridional overturning and due to a spinup of the subpolar gyre. The corresponding subpolar and subtropical heat content changes could in principle act as an immediate positive feedback and a delayed negative feedback to the NAO.

1. Introduction

The mechanisms of natural climate variability on interannual to interdecadal timescales in midlatitudes are of major interest in climate research. Of particular interest is the question whether two-way interactions between ocean and atmosphere exist as these could provide some predictability of climate variations, with potentially considerable socioeconomic benefits.

The focus of this study is on the North Atlantic region where the North Atlantic oscillation (NAO) is the dominant atmospheric mode of natural variability. The NAO was described by Wallace and Gutzler (1981) as a teleconnection pattern in the North Atlantic sector resembling a simultaneous strengthening and weakening of the Iceland low and Azores high. The influence of the NAO on regional climate variability over the North Atlantic and its neighboring continents was described by, for example, Hurrell (1995), its impact on sea surface temperatures (SST) and air–sea fluxes has been documented by, for example, Cayan (1992). Anomalous high heat loss of the subpolar North Atlantic and anomalous heat gain in the subtropical western North Atlantic in a winter of a ''positive'' phase of the NAO with enhanced cold and dry westerlies in the subpolar North Atlantic and reduced offshore winds in the midlatitudes generates a dipole pattern in the SST with cool anomalies in the subpolar North Atlantic and warm anomalies in the midlatitudes. Another cool SST anomaly is located off the west coast of North Africa.

On the other hand, comparably less is known about the impact of the NAO on the North Atlantic Ocean dynamics. It is, however, known that there are long-term changes in the North Atlantic. Bjerknes (1964) found interdecadal changes in the SST in the Gulf Stream–North Atlantic Current region, developing against the local damping influence of the atmosphere. This unusual development and persistence of SST anomalies was also reported by recent studies (Kushnir 1994; Deser and Blackmon 1993). In contrast to the sea surface data, the database of the history of the subsurface North Atlantic is very sparse. Dickson et al. (1996) describe what is known from observations about changes in convection and subsurface water mass structure in the northern North Atlantic and relate these changes to the NAO. Molinari et al. (1997) found decadal fluctuations in the water masses of the upper subtropical North Atlantic Ocean related to the NAO. Curry et al. (1998) tracked signals in water masses formed in the Labrador Sea into the abyssal subtropical gyre (which were also correlated with the NAO), and found a correlation between cooling of Labrador Sea water masses and deep subtropical temperature anomalies with a time lag of 6 yr. Levitus et al. (1994), Houghton (1996), and Reverdin et al. (1997) also showed long-term variability in the North Atlantic, but its causes are not fully understood.

Corresponding author address: Carsten Eden, Institut für Meereskunde an der Universität Kiel, Düsternbrooker Weg 20, D-24105 Kiel, Germany.
E-mail: ceden@ifm.uni-kiel.de

Another way of exploring the subsurface history of the ocean is given by simulations with Ocean General Circulation Models (OGCMs) forced with observed (or taken from reanalysis products) surface flux changes. Häkkinen (1999) analyzed a four-decade integration of a coupled sea–ice sigma-coordinate ocean model of the Arctic and the North Atlantic Ocean. Her model reveals that the thermohaline circulation (THC) and the meridional heat transport (MHT) have increased in the early 1970s and have entered an intense period from the mid-1980s to the end of 1993. The strengthening followed closely the NAO index.

Hence, it seems likely that the North Atlantic responds to atmospheric forcing variability with considerable changes in the horizontal and meridional circulation and with related changes in the heat transport. Bjerknes (1964) already suggested that the observed interdecadal development of persistent SST anomalies in the North Atlantic against the local damping heat fluxes requires the contribution of changes in oceanic heat transport. It is, however, still unclear what mechanisms lead on which timescales to these changes in heat transport.

The capability of midlatitude SST or oceanic heat content anomalies to influence atmospheric variability on interannual timescales has been controversial (Palmer 1996). Rodwell et al. (1999) found that an Atmospheric General Circulation Model (AGCM) forced with SST anomalies produces in an ensemble mean sense the NAO-related pattern in sea level pressure. The SST forcing pattern was, in turn, related to the NAO in the AGCM. There are, however, concerns about the role of the SST forcing in such experiments (Bretherton and Battisti 2000). An impact of SST (heat content) anomalies on the NAO may rise the possibility of decadal-scale feedback mechanisms between ocean and atmosphere. This may give, in turn, some skill for predictability of natural climate variability.

The objective of the present study is to investigate the mechanisms of the interannual to decadal oceanic response to realistic atmospheric forcing in the North Atlantic, especially with respect to the NAO. To this end we use a state-of-the-art OGCM of the North Atlantic. Variable surface forcing is taken from the National Centers for Environmental Protection–National Center for Atmospheric Research (NCEP–NCAR) reanalysis (Kalnay et al. 1996). The results of the model integration driven by the full forcing from the NCEP–NCAR data over four decades show that most of the oceanic variability is correlated to the NAO. The impact of the forcing variability is explored by separately investigating the response to heat flux, wind stress, and freshwater flux variability. Idealized response experiments to high or low NAO phases furthermore clarify the mechanisms of the oceanic response.

2. Models and first results

a. Model configuration

The integrations presented in the following are performed with a non-eddy-resolving model of the Atlantic Ocean. The model OGCM is an enhanced version of the Geophysical Fluid Dynamics Laboratory (GFDL) MOM2.1 code (Pacanowski 1995), developed as part of FLAME, a hierarchy of models for the Atlantic Ocean (Dengg et al. 1999; see, e.g., http://www.ifm.uni-kiel.de/to/FLAME/index.html). The resolution of the present model is $\frac{1}{3}^\circ \cos\phi$ lat $\times$ $\frac{1}{3}^\circ$ long with 45 levels in the vertical. The model domain spans the entire Atlantic from 100°W to 30°E and 70°S to 70°N, however, this study focuses on the North Atlantic. The diffusion terms are harmonic, tracers are mixed along neutral surfaces using a scheme originally developed by Cox (1987). Also included is the eddy-induced tracer advection parameterization of Gent and McWilliams (1990). The northern and southern boundaries and the Gulf of Cadiz of the model are closed with restoring zones for temperature and salinity, whereas the Drake passage and the eastern boundary at 30°E are represented as open boundaries (Stevens 1990) with a prescribed in- and outflow of the Antarctic Circumpolar Current (about 130 *Sv*) and its associated water masses. More details concerning the model configuration are given in Eden and Jung (2000) and Eden (1999).

b. Forcing

To reach a quasi-dynamical equilibrium, the model was forced in a 50-yr-spinup phase with wind stresses and heat fluxes of a monthly climatology from the European Centre for Medium-Range Weather Forecasts (ECMWF; Barnier et al. 1995). The initial condition for potential temperature and salinity were taken from the Levitus and Boyer (1994) monthly climatology.

The heat flux forcing is formulated as a Haney-type (Haney 1971) surface boundary condition:

$$Q = Q_0 + \lambda(T_{\text{clim}} - T_{\text{model}}),$$

that is, a prescribed heat flux Q_0 plus a restoring to a climatological SST (T_{clim}) with a temporally and spatially varying parameter λ, determined from a linearization of the bulk parameterization of the surface heat flux components; λ and T_{clim} are given by Barnier et al. (1995). As a simple parameterization of the effects of sea ice, surface cooling, freshwater fluxes, and fluxes of turbulent kinetic energy are set to zero when the SST is at or below the freezing point in the model, whereas surface heating and the wind stress are not altered. Note, however, that there is no prognostic sea-ice model included in the configuration.

Monthly heat flux anomalies ΔQ_{NCEP} (latent heat flux, sensible heat flux, net longwave and shortwave radiation fluxes taken from the NCEP–NCAR reanalysis for the years 1958–97; anomalies are computed with respect to the long-term annual mean cycle) are added to Q_0 in the subsequent experiments, whereas the climatological SST was not changed. Therefore, the effective heat flux anomalies felt by the model differ from the NCEP–NCAR anomalies:

$$\Delta Q = \Delta Q_{\mathrm{NCEP}} - \lambda \Delta T_{\mathrm{model}},$$

where $\Delta T_{\mathrm{model}}$ denotes the deviation of the modeled SST from a long-term annual mean cycle in the spinup phase of the model. The deviation of ΔQ from ΔQ_{NCEP} remains small, however (except for the tropical Atlantic, which is discussed below).

Note that the flux data from the NCEP–NCAR reanalysis project are biased by errors not only resulting from the typical problems with measurement accuracy and sampling, but also due to inadequacies in the model and/or the parameterizations used in the reanalysis. However, the discussion of these errors is beyond the scope of the present study, but we want to remind the reader that these errors might influence the model results.

We have excluded synoptic atmospheric variability with timescales less than a month in the experiments. However, this variability affects the ocean predominantly by wind-stress variability, with an impact on the barotropic flow (Willebrand et al. 1980; Stammer et al. 2001, manuscript submitted to *J. Phys. Oceanogr.*) and the mixed layer. The impact of the fluctuating barotropic flow by nonlinear effects on the monthly mean circulation is neglected here. The mixed layer is affected by the synoptic wind stress variability via a transfer of turbulent kinetic energy, which is able to deepen the mixed layer. Note that we are using a mixed layer parameterization following Kraus and Turner (1967) in the ocean model for the mean impact of this mechanism. We are, however, neglecting the impact of fluctuations of this input.

Sea surface salinity (SSS) was restored toward the Levitus and Boyer (1994) monthly climatology, freshwater flux anomalies (evaporation minus precipitation, $E - P$, from NCEP–NCAR) are added to the restoring condition term for the SSS in the experiments. We have also performed some integrations with mixed boundary conditions (a fixed surface freshwater flux and unchanged surface heat flux condition) for which the model was integrated from year 40 to 50 with the diagnosed climatological freshwater fluxes of year 40 with the freshwater anomalies being added. In all cases the freshwater flux anomalies (originating from $E - P$ variability in the model domain) were found to be of minor importance for the oceanic response. Therefore, these experiments will not be discussed further on here. Note, however, that we have excluded the possible impact of freshwater forcing variability from outside the model domain, from river runoff changes and from sea-ice variability.

c. First results

The model solution after the spinup phase is in many aspects similar to other OGCMs of the North Atlantic Ocean at such resolutions. Figure 1 shows the mean barotropic streamfunction. The North Atlantic subtropical gyre strength is about 35 Sv (1 Sv = 10^6 m^3 s^{-1}), consistent with observation estimates given, for example, by Schott et al. (1988), the strength of the subpolar gyre is about the same value. Figure 2 shows the mean meridional overturning streamfunction. The maximum strength of the meridional overturning, is about 18 Sv, which is in the expected range for *z*-level North Atlantic models (Willebrand et al. 1999, manuscript submitted to *Progress in Oceanography*; Döscher and Redler 1997; Böning et al. 1996) and also consistent with observational estimates (Römmich and Wunsch 1985). The southward transport (overflow) below $\sigma_\Theta = 27.78$ kg m^{-3} across the Denmark Strait is 2.5 Sv and 1.3 Sv across the Iceland–Scotland sills, which is also consistent with the estimates from observations of the flow rates, for example, given by Dickson et al. (1990). The annual mean meridional heat transport (MHT) has a maximum value of 0.9 PW around 20°N (1 PW = 10^{15} W), which is about 10% lower than the canonical values from the observational estimates given, for example, by MacDonald and Wunsch (1996) (a well-known model deficit) but, however, well within the level of uncer-

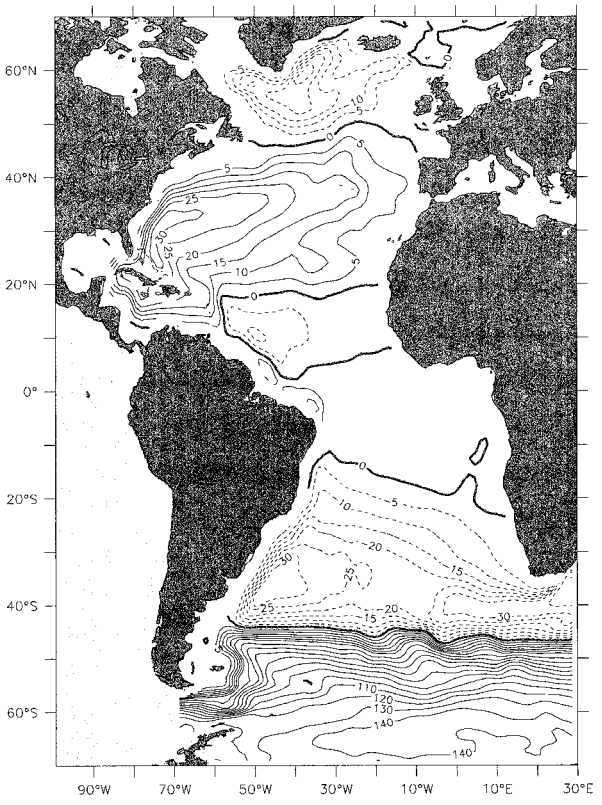

FIG. 1. The annual mean horizontal streamfunction in the coarse-resolution model (Sv). Contour intervals are 10 Sv, and 5 Sv between −30 and 30 Sv. The model data have been smoothed with a spatial 3-point Hanning window prior to contouring to remove grid-scale numerical noise. The figure shows the last year of the spinup in the model.

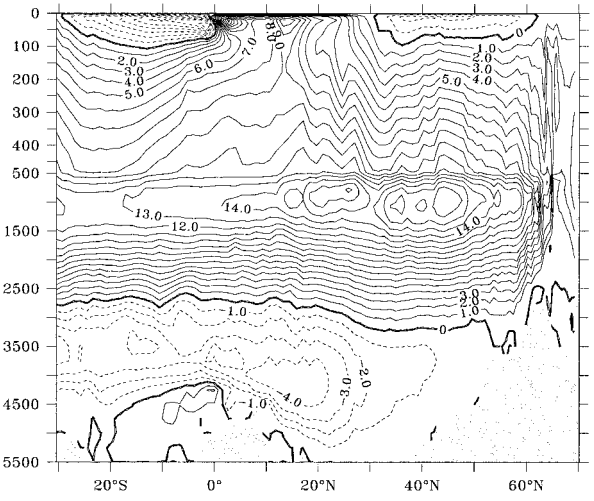

FIG. 2. The annual mean meridional streamfunction in the coarse-resolution model (Sv). The figure shows the annual means of the last year of the spinup in the model. Contour interval is 1 Sv. Note that the upper 500 m are stretched in this figure.

tainties of these estimates. For more details the reader is referred to Eden (1999).

After the spinup phase, the model was forced with interannual variations of heat, freshwater, and momentum fluxes in experiment ref (a complete list of the experiments that are discussed here is given in Table 1). Figure 3 shows the induced changes of the meridional heat transport at 48°N in the model for this experiment. The heat transport fluctuates between about 0.3 and 0.7 PW; prominent signals are for example, the persistent lowering of heat transport during the early 1970s and a rapid increase around 1995/96.

As mentioned above, the bulk of the induced changes in the northern North Atlantic is related to the NAO. To show this (for the heat transport), we will briefly compare here the results of experiment ref with an experiment in which the model was forced with the NAO-related surface flux changes only. This was done, projecting surface flux anomalies (heat, freshwater fluxes, and wind stress) from the NCEP–NCAR reanalysis onto the NAO index (which is taken in the present paper as the difference of normalized sea level pressures between Ponta Delgada, Azores, and Stykkisholmur–Reykjavik, Iceland). A more detailed description of this method and the regression maps is given below and in Eden and Jung (2000). The heat transport at 48°N is shown for the common period of both experiments in Fig. 3. Correlation between both time series is about 0.9. The correlation for the thermohaline circulation (THC) changes (annual means) for both experiments (not shown) is also high, ranging about 0.7–0.8 in the northern North Atlantic.

It is obvious from the figure that the most part of the modeled variability of THC and heat transport near the subpolar front is directly caused by the NAO. Note that

TABLE 1. A complete list of the experiments that are discussed in the text.

Ref	Starting from the spinup the model was integrated 39 yr with momentum fluxes and surface heat fluxes derived from the NCEP–NCAR data
Heat	Same as ref, but interannual heat flux variability only
Wind	Same as ref, but interannual wind stress variability only
NAO-both	Ten year positive NAO scenario, with related changes in heat fluxes and wind stresses
NAO-wind	Same as NAO-both, but with wind stress changes only
NAO-heat	Same as NAO-both, but with heat flux changes only

there is no timescale dependency of the correlation, as coherency spectra reveal (not shown).

Modeled SST anomalies were compared with observations over the 39-yr period taken from Smith et al. (1996). Local correlation maps show similar results as, for example, in Häkkinen (1999) (her Fig. 2). Correlations during wintertime, up to 0.8, are higher than those for the whole year, which are about 0.4–0.7. Obviously, the model performs much better in simulating the deep mixed layer depth temperatures in winter than the shallower ones in summer, in which the representation of the mixed layer dynamics become important. However, there are also regions with less than 0.3 or even insignificant correlations in all seasons in the present integration and also in the integration discussed by Häkkinen (1999). These regions are the shelf of Labrador, the east coast of the United States north of Cape Hatteras, the west coast of North Africa and the equatorial Atlantic. The low correlations indicate certain well-known model deficiencies. Especially the pathway of the Gulf Stream–North Atlantic Current is not well represented at this resolution. The low correlations

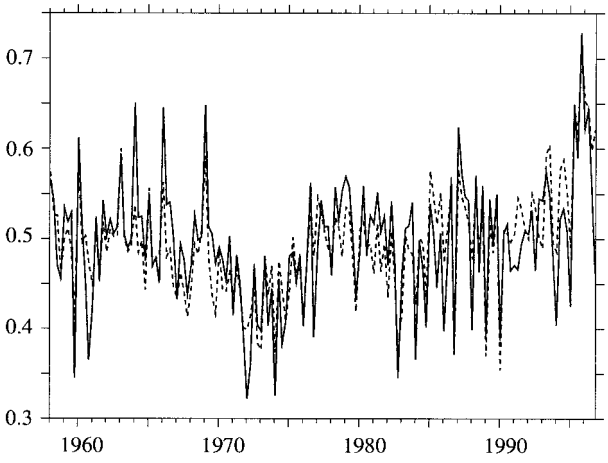

FIG. 3. The meridional heat transport (seasonal means; PW) in experiment REF at 48°N (solid line) and the same variable for an experiment in which the model was forced with NAO-related flux anomalies only (dashed line).

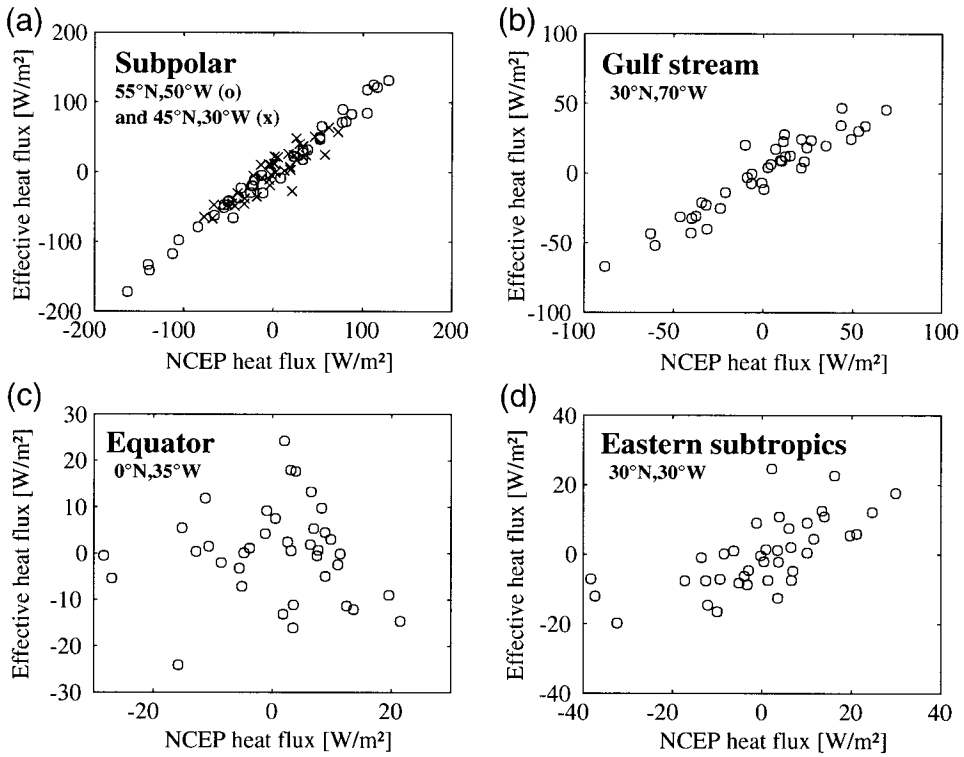

FIG. 4. Local correlations between the wintertime (Jan–Mar) surface heat flux taken from the NCEP–NCAR reanalysis (ΔQ_{NCEP}) and the effective wintertime heat flux felt by the model (ΔQ) at four different locations in the North Atlantic. Note that two different correlations are shown in the upper-left panel; circles denote heat fluxes in the central Labrador Sea, crosses denote heat fluxes near the subpolar front.

along the shelf of Labrador and Greenland indicate the processes that control the sea-ice coverage (or a data-coverage problem in the observations, as noted by Häkkinen (1999); note that her OGCM includes a sea-ice model).

Strong deviations of ΔQ from ΔQ_{NCEP} can be expected in the equatorial Atlantic (Gulev et al. 2000, personal communication and Trenberth 2000, personal communication) since NCEP–NCAR heat fluxes strongly depend here on the parameterization of the hydrological cycle. This can indeed be seen in Fig. 4, showing ΔQ_{NCEP} versus ΔQ at different regions of the North Atlantic. Correlations are 0.99 and 0.9 for the two subpolar regions, 0.94 for the Gulf Stream and 0.68 for the eastern subtropics. Note that no significant correlation was found for the equatorial region. As the focus of the present study is the northern North Atlantic, this model discrepancy is, however, of no further consequence here.

3. Response to interannual heat flux variations

To identify the mechanisms that determine the induced oceanic variability, the forcing by the atmosphere is separated into the variability in heat fluxes (experiment heat) and wind stresses (experiment wind) only. In experiment heat the model was forced with interannual heat flux variability taken from the NCEP–NCAR data, all other surface forcing was taken from the climatology. The response in the horizontal and thermohaline circulation will be described subsequently in this section.

a. Horizontal circulation

Figure 5 shows the leading Empirical Orthogonal Functions (EOFs) of the wintertime heat fluxes (taken from the NCEP–NCAR data) and of the mixed layer depths in experiment heat. It is obvious from the figure that most of the variance in the mixed layer depth is restricted to the Labrador Sea in the leading EOF mode (57.4% explained variance). The deepest mixed layers in the climatological mean are also located in that region (maximal convection reaches down to 2500 m). In the model, strong convection took place in the winters of 1971/72 and 1983/84 and in the early 1990s, while in the 1960s, the late 1970s, and late 1980s convection was anomalously weak. The leading EOF of the surface heat flux (29.2% explained variance) shows increased ocean heat loss in the subpolar North Atlantic that coincides with anomalously deep mixed layers in the Labrador Sea. At the same time the ocean gains anomalous heat in the Gulf stream region. The temporal correlation of both EOF modes is 0.71 (Fig. 5a). A similar heat flux pattern is obtained by a local regression of the time

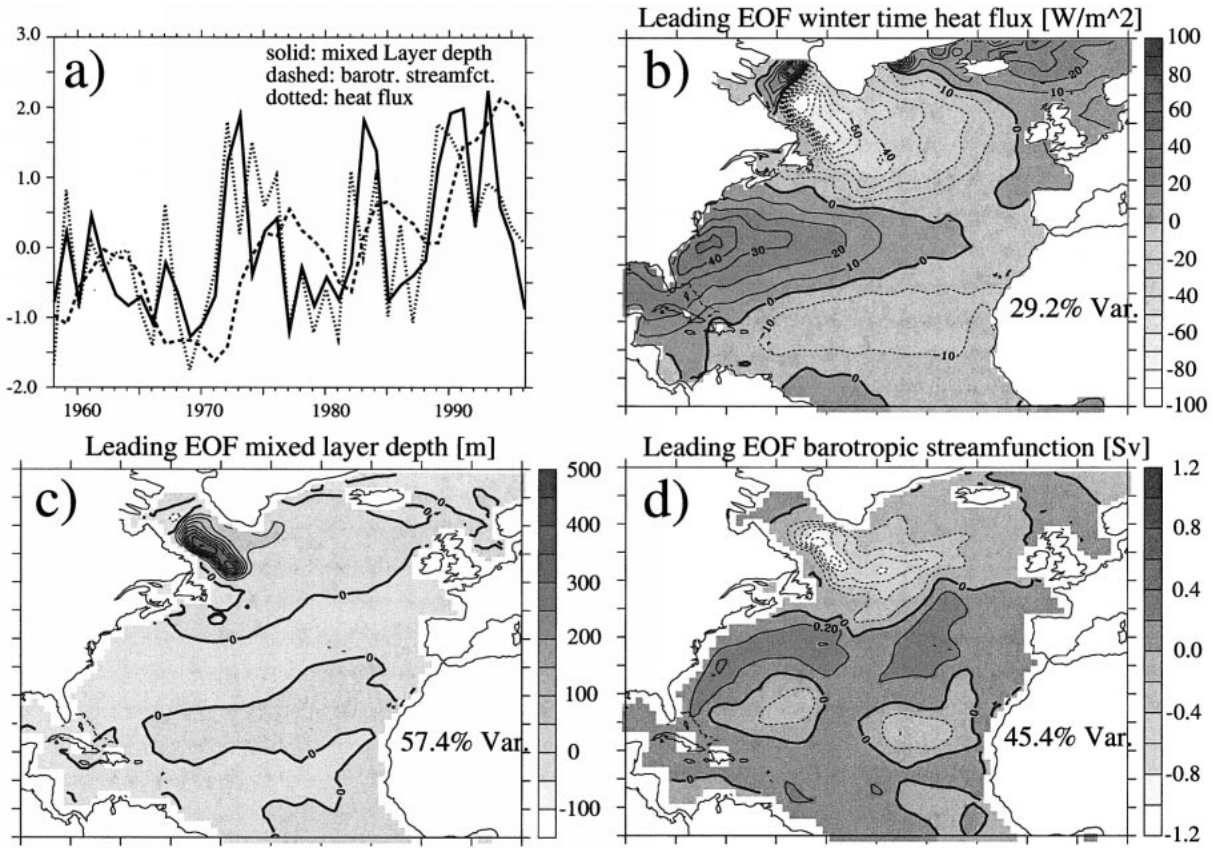

FIG. 5. (a) The principal components of the leading EOFs of the wintertime mixed layer depth (solid) in the experiment heat, the wintertime barotropic transport streamfunction (dashed) in heat, and the heat flux forcing for that experiment (dotted). (b) The leading EOF of the wintertime heat flux anomalies (W m^{-2}). (c) The leading EOF of the wintertime mixed layer depth (m). (d) The leading EOF of the barotropic streamfunction (Sv). None of the time series has been filtered in time. Explained variances are noted in the figures. The EOF of the barotropic streamfunction has been smoothed with a spatial 3-point Hanning window prior to the contouring.

series of the heat fluxes to the NAO index (Cayan 1992). The pattern is caused by stronger westerlies and more advection of cold, dry air masses into the subpolar region during high-NAO phases and by reduced offshore winds over the Gulf Stream area. The temporal correlations of the principal components of mixed layer depth and heat flux with the NAO index are 0.72 and 0.79, respectively.

Figure 5d shows the leading EOF of the horizontal transport streamfunction (45.4% explained variance). The streamfunction is characterized by a cyclonic anomaly in the subpolar gyre and weaker anomalies in the subtropical gyre. A lagged response of the principal components of the horizontal streamfunction to the mixed layer depth anomalies is obvious from Fig. 5a. Following the convection events in the winter 1971/72, 1983/84, and 1989/90, there is an enhancement of the subpolar gyre circulation of about 2 Sv after 2–3 yr. This spinup of the subpolar gyre should be due to the coupling of the baroclinic structure and the barotropic mode in the presence of a sloping topography since there are no variations of wind stress in experiment heat and other coupling terms should be small.

b. Overturning circulation

Figure 6 shows anomalies of the spatially averaged mixed layer depths in the Labrador Sea together with anomalies of a THC index for experiment heat. The THC index (a measure of the strength of the THC) is defined here as the meridional transport streamfunction at 52°N in 1500-m depth. The latitude 52°N was chosen since it is located at the southern end of the convection region in the Labrador Sea. The maximum amplitude of the variations of the meridional streamfunction at 52°N is at about 1500-m depth. (The maximum amplitudes of about 3 Sv of the variations in the streamfunction are located near their time mean maximum at 45°N). It is obvious from Fig. 6 that at periods with strong convection in the Labrador Sea, for example, in the winter 1971/72, 1983/84, or 1989/90, the THC index increases by about 2 Sv. The same response of the THC is obtained by restricting the variable surface heat flux forcing to the Labrador Sea only. This can be seen in Fig. 6 (dashed lines) showing the Labrador Sea convection depths and the THC index for such an experiment.

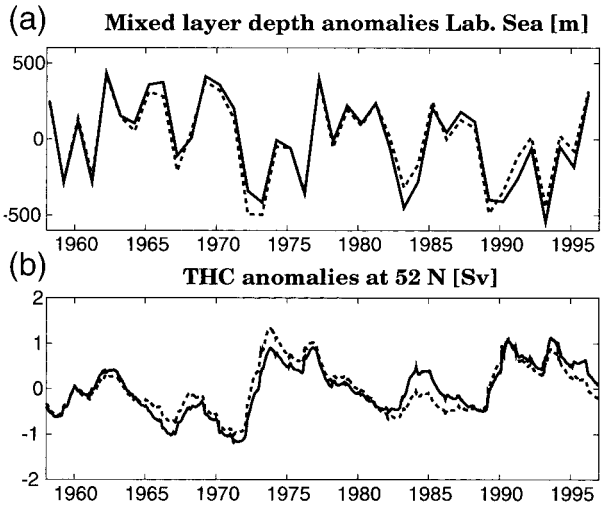

FIG. 6. Anomalies of the wintertime mixed layer depth in the Labrador Sea and the THC index at 52°N in 1500 m for experiment heat (solid lines) and an experiment in which the heat flux variability is restricted to the Labrador Sea only (dashed lines). The Labrador Sea is defined as the region north of 52°N and east of 43°W. Note, that the Hudson Bay and regions north of the Davis Strait are not part of the model domain. The mean mixed layer depth in the Labrador Sea at the end of the winter is about 900 m. The mean of the THC at this latitude is about 12 Sv at 1500-m depth, 500 m below the maximum of 15 Sv.

The mean downwelling in the Labrador Sea region across 1500 m is only about 3 Sv at 1000-m depth, as compared with more than 12 Sv eastward and northward of the Labrador Sea. In contrast, the Labrador Sea region accounts for almost all of the anomalous downwelling north of 52°N in heat (standard deviation 0.5 Sv, as compared with 0.2 Sv elsewhere). Thus, strong convection in the Labrador Sea seems to be a trigger for a lagged enhanced downward motion in the Labrador Sea, in addition to the spinup of the subpolar gyre.

To visualize the basinwide structure of the baroclinic response, we consider the anomaly ΔD of the dynamic height at 100 m relative to 2000 m. Isolines of ΔD serve as streamlines for the differences of the geostrophically balanced flow between 100 and 2000 m and thus can show the zonal location of circulation anomalies that are related to the changes of the THC. In order to determine propagating structures in the data and to estimate the associated timescales (period and *e*-folding decay), a Principal Oscillation Pattern (POP) analysis (Hasselmann 1988; Storch et al. 1988) of the dynamic height anomalies ΔD has been performed.

Figure 7 shows the dominant POP of ΔD in experiment heat. This POP has an estimated period of about 12 yr and an *e*-folding scale of about 15 yr. It describes 55% of the variance and is derived from the annual mean fields, which have been filtered with a 2.5-yr low-pass filter prior to the POP analysis. Figure 7a shows the POP coefficient. Positive (negative) values for the real part and values near zero for the imaginary part of the coefficients, for examples, during the early 1970s, correspond to the positive (negative) spatial structure in Fig. 7b, which is the real part of the POP pattern. Positive (negative) values for the imaginary part and values near zero for the real part of the coefficients correspond to the positive (negative) structure shown in Fig. 7c, which is the imaginary part of the POP pattern.

The figure shows that for a convection event, as, for example, in the winter 1971/72, the POP is in a state similar to Fig. 7b; that is, a negative ΔD resides south of the Labrador Sea region. About 3 yr afterwards, the POP is in a state similar to Fig. 7c (the period is about 12 yr, one-quarter of that period, 3 yr, corresponds to the development between Fig. 7b and Fig. 7c). A positive ΔD has grown in the Labrador Sea while the negative anomaly has propagated into the subtropical gyre. The positive ΔD near the western boundary in Fig. 7c is associated with an enhanced northward transport in the subpolar upper ocean (negative zonal gradient of ΔD corresponds to a positive vertical shear in the meridional velocity; note that the vertical coordinate is oriented positive upward) and thus with enhanced THC in that region. About 6 yr after the convection event, the POP is in a state similar to the negative spatial structure in Fig. 7b, that is, the positive ΔD has propagated southward. After about 9 yr (negative pattern of Fig. 7c) the positive ΔD has propagated into the subtropical gyre.

As shown before in Fig. 6, the convection events in the Labrador Sea are followed by a positive overturning anomaly in the northern North Atlantic with a lag of 2–3 yr. The POP shows that this overturning anomaly is located in the Labrador Sea and begins to propagate into the subtropical gyre along the western boundary with a timescale of about 6–9 yr. The propagation resembles a first baroclinic mode Kelvin or topographic Rossby wavelike response to the convection changes in the Labrador Sea, whereas the timescale of the propagation seems to be too long for such a mechanism.

Similar propagating structures on such long timescales have been described previously in OGCMs of different horizontal resolution: Döscher et al. (1994) found a considerably faster response to subpolar buoyancy changes in a higher-resolution model (⅓°). They argued that the horizontal scales of baroclinic Kelvin waves are not resolved in coarse-resolution models (coarser than 0.3°–0.5°). However, there is still a boundary wave in coarse-resolution models equivalent to a Kelvin wave but with a considerable slower phase velocity. Gerdes and Köberle (1995) point to the importance of advection of density anomalies within the Deep Western Boundary Current. On the other hand, Greatbatch and Peterson (1996) noted the retarding influence of a weak stratification in the subpolar region to the baroclinic boundary waves. However, the mechanism for the described propagating structure in the present model remains uncertain since experiments (not shown) including a tracer release in the Labrador Sea show a

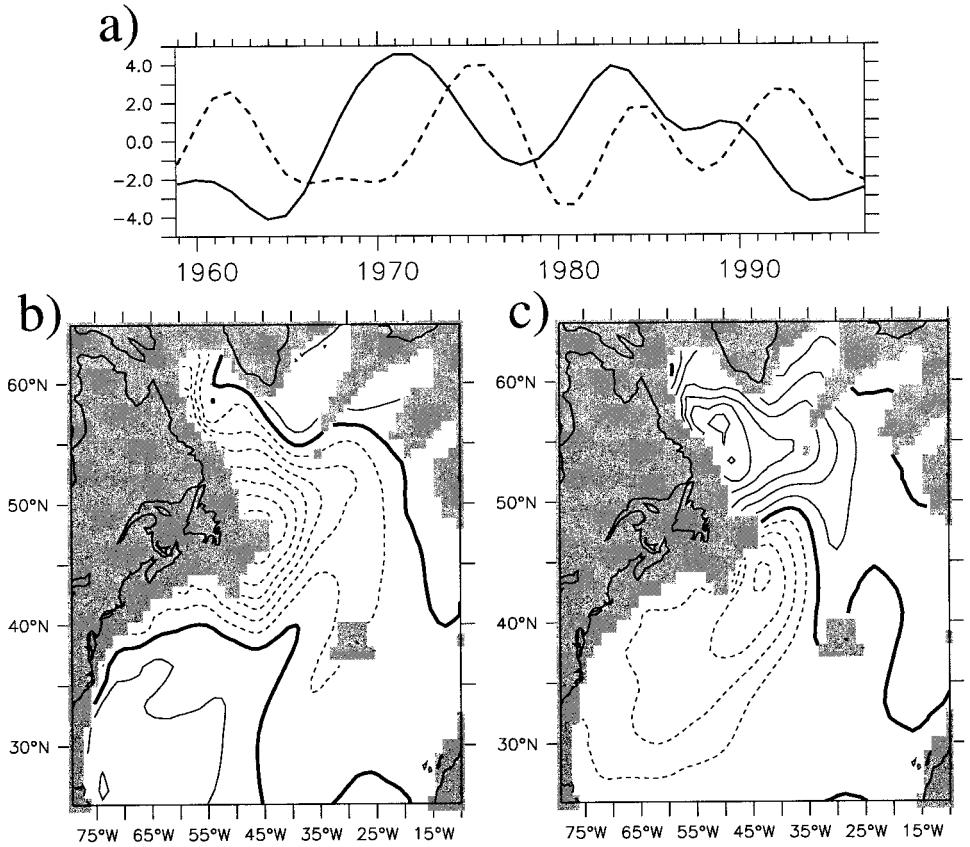

FIG. 7. The dominant POP of the dynamic topography anomalies in experiment heat. (a) The POP coefficient. The real part of the coefficient ($m^2\ s^{-2}$) is denoted by the solid line, the imaginary part by the dashed line. (b) The real part of the spatial structure of the POP. (c) The imaginary part of the spatial structure of the POP. Contour interval is 0.01 for (b) and (c); dashed lines denote negative values. The estimated period of the POP is 12 yr, the *e*-folding decay timescale is 15 yr, and it explains 55% of the total variance.

slightly higher advection timescale than the timescale of the POP and the phase velocity of the Kelvin wave is still too small despite the weak stratification in the subpolar North Atlantic.

4. Response to interannual wind stress variations

In experiment wind, the model was forced with interannual wind stress variability (monthly mean anomalies) taken from the NCEP–NCAR data; all other forcing was climatological as in the spinup integration. To relate the wind stress forcing to the response of the circulation of the model, results of a Canonical Correlation Analysis (CCA) following Barnett and Preisendorfer (1987) will be shown below. The CCA deals with two multivariate time series (in our case the wind stress forcing and the oceanic circulation) and detects the patterns in both time series that share maximum correlation of their coefficients (the canonical correlation coefficients). Here, the CCAs are performed with different lags between the atmospheric forcing and the oceanic response to distinguish between immediate and lagged response.

a. Horizontal circulation

Figures 8a and 8b show the leading patterns of a CCA between the wind stress curl and the barotropic streamfunction in experiment wind. Both time series have been detrended and filtered with a 2-yr low pass. The instantaneous oceanic barotropic response (25% explained variance) to the leading pattern in the wind stress curl (30% explained variance) is an anticyclonic circulation anomaly centered around about 40°N and 40°W. The amplitude of the circulation anomaly is about 1.2 Sv for the amplitude in the wind stress curl pattern shown in Fig. 8b. Note that this wind stress curl pattern is similar to a pattern obtained by a regression to the NAO index and is also similar to the leading EOF of the wind stress curl (both not shown). The corresponding canonical correlation coefficients (Fig. 9) are also correlated to the NAO index (0.70), which is also shown in Fig. 9. A regression of the NAO index to the barotropic streamfunction resembles also a pattern as in Fig. 8a (not shown). Thus, the barotropic response to the dominant interannual variability pattern in the atmosphere, which is the NAO, is given by Fig. 8a.

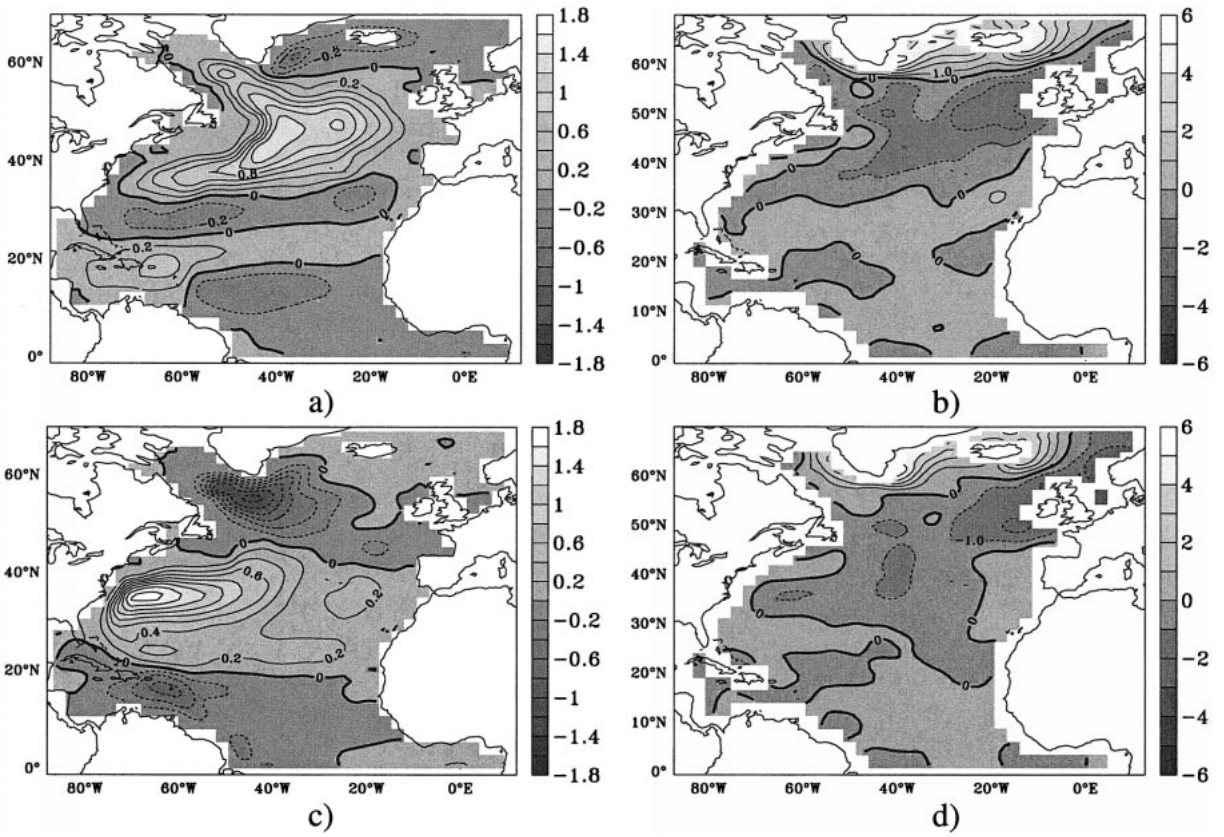

FIG. 8. The CCA patterns of wind stress curl (10^{-6} N m^{-3}) and barotropic streamfunction (Sv) of experiment wind with lag 0 and 3-yr lag (atmosphere leads). (a) CCA pattern of barotropic streamfunction at lag 0. This pattern explains 25% variance of the time series. (b) CCA pattern of wind stress curl at lag 0 (30% explained variance). (c) CCA pattern of barotropic streamfunction at 3-yr lag (24% explained variance). (d) CCA pattern of wind stress curl at 3-yr lag (25% explained variance). Both time series have been detrended and filtered with a 2-yr low pass. The CCAs have been performed using the first five principal components of an EOF analysis (88% and 75% explained variance for the barotropic streamfunction and wind stress curl, respectively). The resulting patterns have been transformed back afterward. The CCA patterns of the barotropic streamfunction have been smoothed with a spatial 3-point Hanning window prior to the contouring. Note that the patterns in the upper row and the lower row are related in pairs, respectively. The upper row shows the immediate response of the ocean in (a) its horizontal circulation (b) to the related pattern in the wind stress curl. The lower row shows the (c) delayed oceanic response to (d) the pattern in the wind stress curl.

Assuming that there are no fast changes in the deep vertical velocities, a simple (topographic) Sverdrup balance holds for the anomalies of the streamfunction on intraseasonal timescales. This balance might explain the pattern of the fast barotropic response. Note, that it is essential for the structure of the response pattern that the wind stress curl pattern (Fig. 8b) is very similar to the time mean pattern shifted by about 10° to the north. Since the forcing pattern is shifted to the north, the oceanic response is shifted as well. Thus, the anticyclonic anomaly in Fig. 8a resembles the (shifted) subtropical gyre in a simple (topographic) Sverdrup balance for the time mean forcing.

To show the delayed response of the horizontal circulation in the North Atlantic, a CCA was performed between the wind stress curl and the barotropic streamfunction with a lag of 3 yr (atmosphere leads). The results are shown in Figs. 8c and 8d and the corresponding canonical correlation coefficients in Fig. 9. The patterns and coefficients for the wind stress curl (25% explained variance) are roughly similar to the ones of the CCA with zero lag, but for 3-yr lag the pattern of the barotropic streamfunction (24% explained variance) now becomes more similar to the time mean of that variable. The amplitude of the anomaly is about 1.2 Sv in the subpolar North Atlantic for an amplitude of one standard deviation in the forcing function. Thus, 3 yr after 1 yr with positive (negative) NAO index the oceanic response is an enhanced (reduced) mean state. The mechanism is very likely associated with baroclinic wave adjustment that also leads via an interaction between baroclinic and barotropic modes in the presence of topography to a slow adjustment of the barotropic mode, as discussed by Anderson et al. (1979).

b. Overturning circulation

The THC response to changes in the atmospheric circulation was also investigated by means of a CCA, now

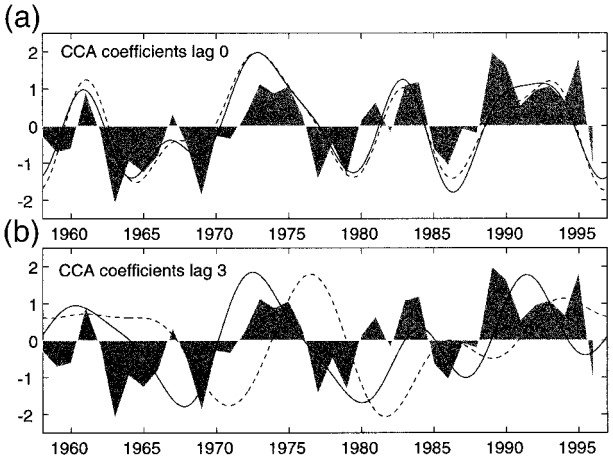

FIG. 9. The CCA coefficients of wind stress curl (solid) and barotropic streamfunction (dashed) of experiment wind at (a) lag 0 and (b) lag 3 yr (atmosphere leads). The correlations are 0.975 and 0.956. The CCAs have been performed using the first five principal components of an EOF analysis (88% and 75% explained variance for the barotropic streamfunction and wind stress curl, respectively). The resulting patterns have been transformed back afterward. Superimposed is the wintertime (Jan–Mar) NAO index (shaded).

computed for the SLP and the THC index (a CCA between wind stress curl and THC index gives similar results; we use SLP here to show also the SLP pattern). Both time series have been detrended and filtered with a 2-yr low pass. Figure 10 shows the dominant patterns of a CCA between SLP and the THC index. Both patterns of SLP (Figs. 10b and 10d, 41% and 20% explained variance) are similar to a local regression with the NAO index (not shown): a dipole with a minimum near Iceland and a maximum near the Azores. The canonical correlation coefficients are also correlated (0.7) to the NAO index. The instantaneous response of the THC (Fig. 10a, 32% explained variance) shows a negative anomaly in the north and a positive anomaly in the south and downwelling near 40°N. The minima and maxima in the THC-index variations are reached within the uppermost model level and there is a nearly linear decrease with depth. Thus, these THC anomalies are caused by the variability in the meridional Ekman volume transport related to the SLP pattern and resulting zonal wind stress anomalies.

Figure 10c shows the 3-yr lagged response of the THC (30% explained variance) to an SLP anomaly shown in Fig. 10d. The SLP pattern and time series (Fig. 10d and Fig. 11) are again very similar to those obtained by the CCA without lag. However, the THC now shows a completely different pattern; a negative anomaly in the south and a positive anomaly in the north and upwelling near 45°N. The maxima and minima are reached at about 500- to 1000-m depth, thus the delayed response must be baroclinic in nature.

To conclude, Fig. 10a shows the instantaneous response of the THC to the NAO, which is dominated by the changes in the Ekman transport at the surface, while Fig. 10c shows the lagged, baroclinic response to the NAO.

5. Response to idealized forcing

The previous sections show, that most of the oceanic variability was induced by changes in heat flux and wind stress related to the NAO. In this section, the oceanic response to persistent high- (or low-) NAO phases is discussed to confirm and strengthen the previous results.

Monthly regression patterns of the heat flux and wind stress time series from the NCEP–NCAR data to the NAO index were used to reconstruct NAO-like forcing patterns. These patterns were multiplied by three standard deviations (of the NAO index) and switched on immediately at the beginning of each experiment. Note, that three standard deviations of the wintertime NAO index have been reached several times within the last decades. Moreover, an increase (or decrease) of the NAO index of several standard deviations from one winter to the next is not an unusual situation. A persistent, constantly high NAO index over several years is, however, an idealized scenario, which is used here to study the oceanic response in absence of other atmospheric variability. Three experiments with different forcing changes were performed (compare also the list of experiments in Table 1). The model was forced with heat flux anomalies from the regression patterns in experiment NAO-heat; all other forcing functions remain the same as in the spinup. Experiment NAO-wind includes only changes in the wind stress forcing, while experiment NAO-both includes both changes in heat flux and wind stress forcing. An experiment equivalent to NAO-both, but with forcing changes related to a negative NAO (again three standard deviations) was performed to study a possible nonlinear oceanic response.

The regression patterns are already described by, for example, Cayan (1992) and are only briefly discussed here. The wintertime heat flux pattern resembles the leading EOF mode of the heat flux (Fig. 5b). The pattern in summer has less clear structure, lower amplitude, and less explained variance. The patterns explain more variance in winter than in summer. The wind stress patterns are similar to the climatological mean in the North Atlantic (north of about 30°N), with the difference that the line of 0 crossing in the zonal wind stress has moved from about 30°N in the mean to about 40°N in the regressions. The patterns explain more variance in winter (up to 60%) than in summer, although the structure of the vector fields are similar. The amplitude of the wind stress vectors reaches at maximum 25% of the climatological mean in winter and about 15% in summer.

a. Circulation and heat transport changes

The circulation changes in NAO-both, NAO-heat, and NAO-wind essentially confirm the previous results. All these circulation changes leave their fingerprints on the

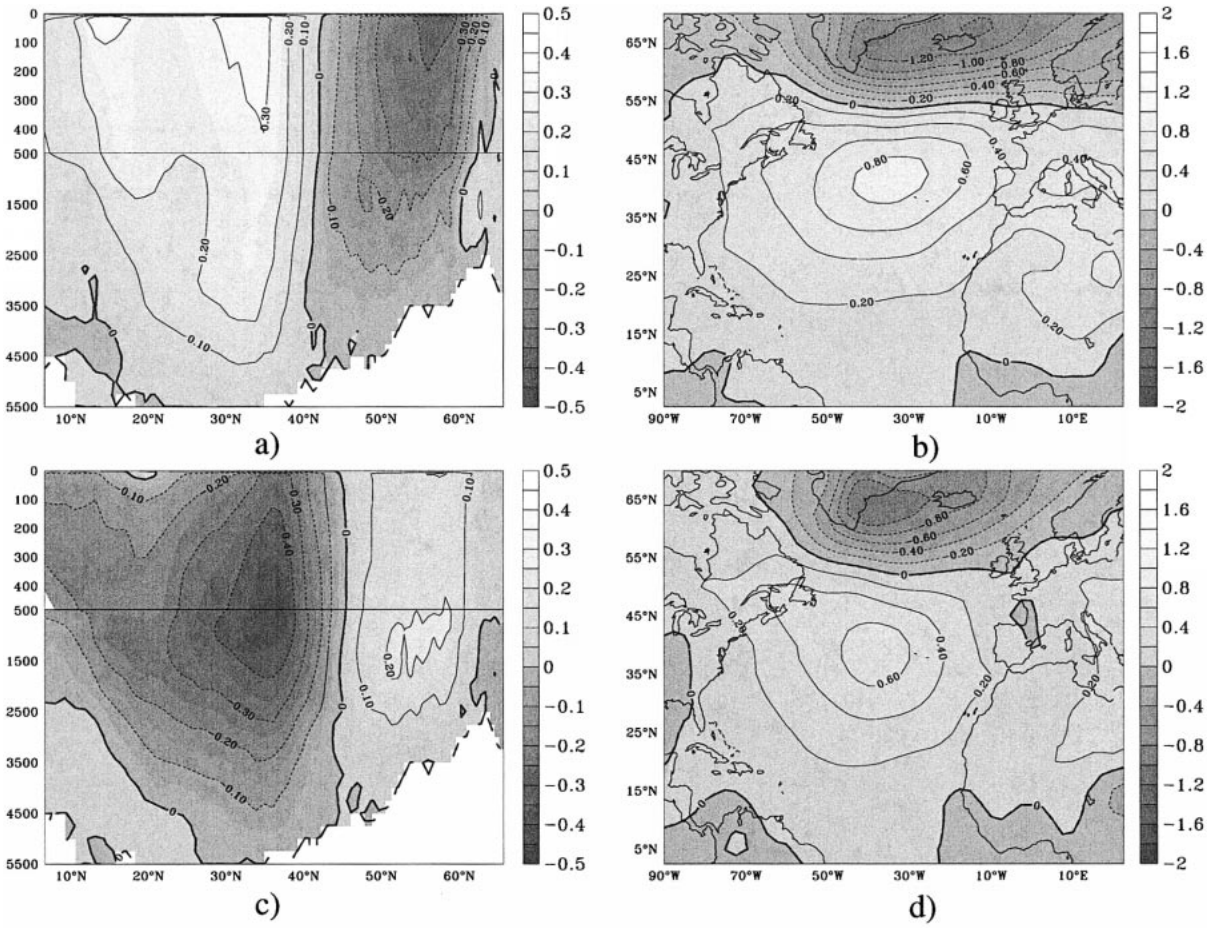

FIG. 10. The CCA patterns of sea level pressure (hPa) and THC (Sv) of experiment wind at lag 0 and lag 3 yr (sea level pressure leads). (a) CCA pattern of THC at lag 0. This pattern explains 32% variance of the time series. (b) CCA pattern of the sea level pressure at lag 0, which describes 41% variance. (c) CCA pattern of THC at 3-yr lag (30% explained variance). (d) CCA pattern of the sea level pressure at 3-yr lag (20% explained variance). Both time series have been detrended and filtered with a 2-yr low pass. The CCAs have been performed using the first five principal components of an EOF analysis (92% and 76% explained variance for the barotropic streamfunction and wind stress curl, respectively). The resulting patterns have been transformed back afterward. Note that the first 500 m are stretched in this figure for the patterns of the THC.

oceanic meridional heat transport (MHT), which could be important for a possible oceanic forcing of the atmosphere. Figure 12 shows the changes in heat transport near the subpolar front at 48°N for the three experiments with NAO-like forcing anomalies. The *overall* response in the MHT of NAO-both (Fig. 12c) solid line) is an immediate reduction of about 10%, and an increase over 20 yr toward an enhancement of about 10%. To relate this change in the heat transport to the changes in the horizontal and thermohaline circulation, the traditional (though not unique) decomposition of the MHT into ''gyre component'' (Fig. 12a) and ''overturning component'' (Fig. 12b) has been made (Bryan 1962). Gyre and overturning component changes will be compared with the changes in the circulation.

In experiment NAO-wind the barotropic streamfunction immediately responds with an anticyclonic anomaly centered at 40°W and 40°N (not shown), very similar to the immediate response in experiment wind (Fig. 8a). The anomaly with an amplitude of 7–8 Sv is recurring every winter. Note, that this *Sverdrupian* response to the wind stress change leads to an anomalous northward transport in the west and an anomalous southward transport in the east, which leads, in turn, together with the positive zonal temperature gradient at the subpolar front to a southward heat transport anomaly. Thus, this barotropic circulation change leads obviously to the immediate reduction of the MHT near the subpolar front, which can also be seen in Fig. 12a (dotted line).

The baroclinic adjustment of the horizontal streamfunction (also not shown) in that experiment is also similar to experiment wind. This adjustment is more or less completed after 6–8 yr and resembles the pattern found previously in wind (Fig. 8c) with an amplitude of 7–8 Sv of the gyre strength changes. The baroclinic adjustment of the barotropic mode (roughly a spinup of

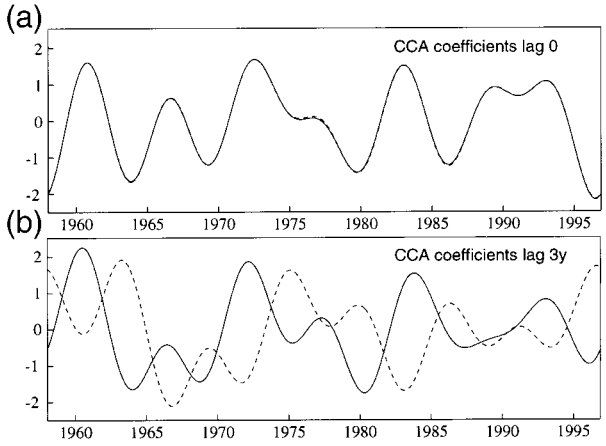

FIG. 11. The CCA coefficients of sea level pressure and THC of experiment wind at lag 0 and lag 3 years (sea level pressure leads). (a) The coefficients of sea level pressure (solid) and THC (dashed) at lag 0 (correlation is 0.998). (b) The coefficients of sea level pressure (solid) and THC (dashed) at lag 3 yr (correlation is 0.940). Both time series have been detrended and filtered with a 2-yr low pass. The CCAs have been performed using the first five principal components of an EOF analysis (92% and 76% explained variance for the barotropic streamfunction and wind stress curl, respectively). The resulting patterns have been transformed back afterward.

both gyres) contributes in minor parts to the increase in MHT after several years near the subpolar front (compare Fig. 12a, dotted line).

In experiment NAO-heat the barotropic streamfunction shows a spinup of the subpolar gyre (about 5 Sv as a response to the change in heat flux forcing, which is completed after about 8 years, very similar to the results from experiment heat (Fig. 5d). This spinup of the subpolar gyre leads to an enhancement of the MHT near the subpolar front, as seen in Fig. 12a (dashed line). Note that NAO-heat lacks a fast barotropic response in the circulation.

In experiment NAO-wind, the immediate response in the THC index (not shown) resembles the leading CCA mode (no lag) of the THC in experiment wind (Fig. 10a). The delayed response (after 5 yr) in NAO-wind is similar to Fig. 10c, if the direct influence of the Ekman volume transport is removed (not shown). Figure 12b (dotted line) shows that the changes in the overturning circulation in NAO-wind contribute in minor parts to the immediate reduction and the delayed enhancement in the heat transport.

There is an increase of about 2.5 Sv of the THC index (at 48°N and 1500 m) during the first 8 yr of experiment NAO-heat. After that initial increase, the THC index decreases slightly again and converges toward a value of 1.5 Sv above the initial value at this position. Figure 12b (dashed line) shows that this increase in the THC contributes also to the delayed increase in the heat transport near the subpolar front.

The Ekman transport change contributes little to the MHT change at 48°N, although there is surely a southward transport anomaly caused by the westerly wind stress anomaly related to the high NAO. This anomaly contributes to the immediate reduction in the overturning component in NAO-wind (Fig. 12b, dotted line). Note that almost no influence of the Ekman transport change can be seen in the gyre component, which is to be explained by the weak zonal dependency of the zonal wind stress anomaly at 48°N. The reduced total heat transport at the subpolar front is therefore predominantly induced by the Sverdrup-like response due to the wind stress change.

In the subtropical North Atlantic, the northward enhanced Ekman heat transport due to a positive NAO raises the total heat transport by up to 0.08 PW in experiment NAO-both. After about 5 yr the anomaly is reduced to 0.04 PW; after 10 yr it is again enhanced to 0.08 PW. This temporal behavior can be explained by the different response of the THC to the anomalies of heat flux and wind stress in the subtropical North Atlantic (note that the gyre component of the heat transport is very small in the subtropics). For experiment NAO-heat there is a slow increase in the strength of the overturning associated with the baroclinic boundary wave response to enhanced convection in the Labrador Sea. For experiment NAO-wind there is an immediate increase in the THC due to enhanced (northward) Ekman transports and a slow decay of the anomalies, which are associated with the baroclinic response of the overturning due to wind stress changes (Fig. 10c). Hence, both

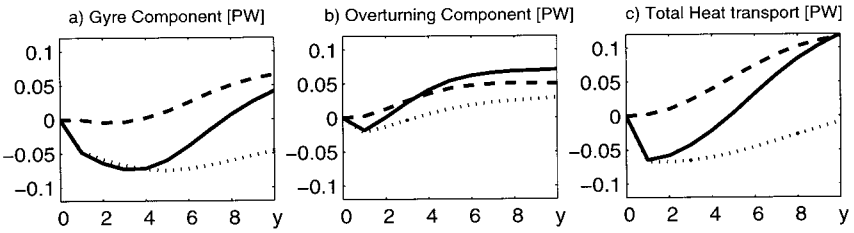

FIG. 12. Changes of MHT (annual means) at 48°N for three different experiments: (a) gyre component of MHT for NAO-both (thick solid), NAO-heat (dashed), and NAO-wind (dotted) (PW). (b) MHT due to overturning for the same three experiments. (c) Total MHT (PW). Note that the annual mean MHT of the last year of the spinup (which is about 0.57 PW) was subtracted from each time series. The overturning component contributes by about 0.35 PW to the annual mean MHT.

responses together show an immediate increase followed by a slight reduction and a further increase in overturning and heat transport changes for experiment NAO-both.

An experiment equivalent to NAO-both, but with surface flux changes related to a negative NAO, reveals that the response is nearly the same but with opposite sign. Hence, the oceanic response to the NAO is symmetric in the model, a nontrivial result since changes in the highly nonlinear process of convection are involved.

b. Aspects of observed short-term oceanic response

The winter 1995/96 shows a pronounced drop of the observed NAO index. Observations have shown a short-term response of the ocean related to this event, which now can be compared with the modeled oceanic response to the NAO.

Bersch et al. (1999) found a shift of the subpolar front in an annually repeated hydrographic section between Ireland and Greenland. Until 1995 the eastern limits of the subpolar gyre were found to be located around 24°W on this section. In 1996, the shallow low-salinity subpolar water disappeared from the waters east of the Reykjanes ridge, to be replaced with the more saline water of the North Atlantic Current. In the model there is also a pronounced shallow saltening and warming around 55°N and 30°W (not shown) in response to a low NAO (in experiment ref as well as in the idealized experiments such as NAO-both). This saltening is caused by the Sverdrup response to the wind stress change: the immediate response to a low NAO is a cyclonic circulation anomaly with its center at the subpolar front, which advects salty and warm water across the subpolar front in the eastern part of the subpolar gyre. Thus, there is a northwestward shift of the subpolar front in the eastern subpolar North Atlantic (and a southeastward shift of the front in the western part).

Reverdin et al. (1999) found a rapid increase of the upper-ocean heat content along a (nearly) monthly repeated section from Iceland to Newfoundland for the winter 1995/1996. Since the increase in heat content was twice as large than what results from local air–sea heat fluxes, they conclude that the remaining part must result from advection of heat content anomalies. Hence, the immediate change in the heat transport due to the Sverdrup response is also consistent with Reverdin et al. (1999).

From the hydrographic sections along the WOCE A2-line Lorbacher (2000), Koltermann et al. (1999) have estimated that in 1997 the heat transport at 48°N has decreased by more than 60% when compared with the preceding year. They suggest that this decrease was related to a fast oceanic response to the drop in the NAO the year before. Note, that this hypothesis is not validated by our model results, which suggest a rapid increase of the heat transport for the same year on the NAO drop as the fast oceanic response.

6. Concluding discussion

The dominant part of the North Atlantic variability generated by variable atmospheric forcing is related to the NAO (well above 90% of the variance of THC and heat transport in the subpolar region) in our set of ocean model experiments. The principal oceanic response to the NAO is summarized in Fig. 12:

- Wind stress associated with a high NAO causes immediately an anticyclonic circulation anomaly centered near the subpolar front, resembling a simple (topographic) Sverdrup balance. This fast response substantially reduces the oceanic heat transport near the subpolar front (Fig. 12a dotted line). The delayed response to the wind stress change is an increase of both the subpolar and the subtropical gyre strength after about 3 yr, due to a baroclinic adjustment, which leads to a delayed small increase in heat transport.
- The immediate response of the THC to a wind stress change related to a high NAO is associated with a change in the Ekman transport and causes a negative anomaly in the subpolar and a positive one in the subtropical region, that is, anomalous downwelling near 40°N. This leads to a minor contribution to the fast reduction of the heat transport near the subpolar front (Fig. 12b dotted line). For the delayed response of the THC to a wind stress change, the signs of the anomalies are reversed. The spatial structure is baroclinic, in contrast to the immediate response, and corresponds to a delayed enhancement of the heat transport.
- Ocean heat loss related to a positive NAO enhances the convection activity in the Labrador Sea, which leads to a strengthening of the subpolar gyre after about 3 yr and a corresponding enhancement of the northward heat transport (Fig. 12a dashed line).
- Enhanced convection activity in the Labrador Sea, induced by ocean heat loss related to a high NAO, is followed by anomalous downwelling located in that region and thus an enhanced subpolar THC after a lag of 2–3 yr. This delayed response in the THC enhances the heat transport (Fig. 12b dashed line). The convection events induce a baroclinic boundary wave-like structure, traveling southward into the subtropical gyre in about 6 yr, leaving enhanced THC behind its wave crest.

As a caveat, the possibility remains that variations in the strength or water mass properties of the overflow of dense water over the northern sills would modify the preceding results. Our model integrations cannot address this issue since they do not include the effect of variations in surface forcing north of the sills. Recent observations and compilations of historic hydrographic observations might suggest that the strength of the over-

flow and its water mass properties remain relatively constant (Dickson et al. 1990; Dickson and Brown 1994). On the other hand, Bacon (1998) analyzed hydrographic sections off Greenland and concludes that there is evidence for decadal variations in the overflow. Thus, we cannot exclude that variability in surface flux changes in the Arctic may have an impact on the large-scale circulation changes in the North Atlantic.

It is interesting to speculate about the signature of a possible atmospheric reaction to the induced oceanic variability. Enhanced (reduced) oceanic heat transport near the subpolar front at about 48°N leads to an anomalous warm (cold) subpolar North Atlantic and anomalous cold (warm) subtropical North Atlantic. That dipole pattern is believed to act most effectively in return on the atmosphere, as suggested by recent studies using AGCMs (Rodwell et al. 1999; Mehta et al. 2000; Latif et al. 2000). Therefore, changes in heat transport near the subpolar front may be important for an active oceanic role in the NAO, and thus for the coupled atmosphere–ocean system in the North Atlantic. For a high-NAO scenario, the immediate decrease of the heat transport near the subpolar front together with the enhancement of the heat transport south of 40°N as a response to a change in wind stress would provide an instantaneous positive feedback on the NAO. After several years, the baroclinic oceanic response enhances the heat transport throughout the North Atlantic warming the subpolar North Atlantic (while the subtropics remain in an indifferent state), which would provide a delayed negative feedback on the NAO.

The foregoing results suggest the possibility of a coupled feedback loop with an interannual to subdecadal timescale in the North Atlantic that might explain the (albeit small) positive correlation of NAO in subsequent years. However, this hypothesis remains to be proven under the presence of a realistic noise level from both the ocean and the atmosphere with the aid of a coupled GCM.

Acknowledgments. We greatly acknowledge the FLAME group, especially the work of R. Redler, for model development. NCEP–NCAR reanalysis data were provided through the NOAA Climate Diagnostics Center (http://www.cdc.noaa.gov/). This is a contribution of the Sonderforschungsbereich 460 ''Dynamics of Thermohaline Circulation Variability'' at the University of Kiel (http://www.ifm.uni-kiel.de/general/sfb460-e.html) supported by the German Research Foundation.

REFERENCES

Anderson, D., K. Bryan, A. Gill, and R. Pacanowski, 1979: The transient response of the North Alantic: Some model studies. *J. Geophys. Res.,* **84,** 4795–4815.

Bacon, S., 1998: Decadal variability in the outflow from the Nordic seas to the deep Atlantic Ocean. *Nature,* **394,** 871–873.

Barnett, T., and R. Preisendorfer, 1987: Origins and levels of monthly and seasonal forecast skill for United States surface air temperature determined by canonical correlation analysis. *Mon. Wea. Rev.,* **115,** 1825–1850.

Barnier, B., L. Siefridt, and P. Marchesiello, 1995: Thermal forcing for a global ocean circulation model using a three-year climatology of ECMWF analysis. *J. Mar. Sys.,* **6,** 363–380.

Bersch, M., J. Meincke, and A. Sy, 1999: Interannual thermohaline changes in the northern North Atlantic 1991–1996. *Deep-Sea Res. II,* **46,** 55–75.

Bjerknes, J., 1964: Atlantic air sea interaction. *Adv. Geophys.,* **10,** 1–82.

Böning, C., F. Bryan, W. Holland, and R. Doescher, 1996: Deep-water formation and meridional overturning in a high-resolution model of the North Atlantic. *J. Phys. Oceanogr.,* **26,** 1142–1164.

Bretherton, C., and D. Battisti, 2000: An interpretation of the results from atmospheric general circulation models forced by the time history of the observed sea surface temperature distribution. *Geophys. Res. Lett.,* **27,** 767–770.

Bryan, K., 1962: Measurements of meridional heat transport by ocean currents. *J. Geophys. Res.,* **67,** 3403–3414.

Cayan, D., 1992: Latent and sensible heat flux anomalies over the northern oceans: The connection to monthly atmospheric circulation. *J. Climate,* **5,** 354–369.

Cox, M., 1987: Isopycnal diffusion in a *z*-coordinate ocean model. *Ocean Modelling,* **74,** 1–5.

Curry, R., M. McCartney, and T. Joyce, 1998: Oceanic transport of subpolar climate signals to mid-depths subtropical waters. *Nature,* **391,** 575–577.

Dengg, J., C. Böning, U. Ernst, R. Redler, and A. Beckmann, 1999: Effects of an improved model representation of overflow water on the subpolar North Atlantic. *WOCE Newsletter,* **37,** 10–15.

Deser, C., and M. Blackmon, 1993: Surface climate variability over the North Atlantic Ocean during winter: 1900–1989. *J. Climate,* **6,** 1743–1753.

Dickson, R., and J. Brown, 1994: The production of North Atlantic Deep Water: Sources, rates and pathways. *J. Geophys. Res.,* **99,** 12 319–12 341.

——, E. Gmitrowicz, and A. Watson, 1990: Deep-water renewal in the northern North Atlantic. *Nature,* **344,** 848–850.

Dickson, R. R., J. Lazier, J. Meincke, P. Rhines, and J. Swift, 1996: Long-term coordinated changes in the convective activity of the North Atlantic. *Progress in Oceanography,* Vol. 38, Pergamon, 241–295.

Döscher, R., and R. Redler, 1997: The relative influence of North Atlantic overflow and subpolar deep convection on the thermohaline circulation in an OGCM. *J. Phys. Oceanogr.,* **27,** 1894–1902.

——, C. Böning, and P. Herrmann, 1994: Response of circulation and heat transport in the North Atlantic to changes in thermohaline forcing in northern latitudes: A model study. *J. Phys. Oceanogr.,* **24,** 2306–2320.

Eden, C., 1999: Interannual to interdecadal variability in the North Atlantic Ocean. Ph.D. thesis, Christian-Albrecht-Universität Kiel, 123 pp.

——, and T. Jung, 2000: North Atlantic interdecadal variability: Oceanic response to the North Atlantic oscillation (1865–1997). *J. Climate,* **14,** 676–691.

Gent, P., and J. McWilliams, 1990: Isopycnal mixing in ocean circulation models. *J. Phys. Oceanogr.,* **20,** 150–155.

Gerdes, R., and C. Köberle, 1995: On the influence of DSOW in a numerical model of the North Atlantic general circulation. *J. Phys. Oceanogr.,* **25,** 2624–2642.

Greatbatch, R., and K. Peterson, 1996: Interdecadal variability and oceanic thermohaline adjustment. *J. Geophys. Res.,* **101,** 20 467–20 482.

Häkkinen, S., 1999: Variability of the simulated meridional heat transport in the North Atlantic for the period 1951–1993. *J. Geophys. Res.,* **104,** 10 991–11 007.

Haney, R., 1971: Surface thermal boundary condition for ocean circulation models. *J. Phys. Oceanogr.,* **1,** 79–93.

Hasselmann, K., 1988: PIPs and POPs: The reduction of complex

dynamical systems using Principal Interaction and Oscillation Patterns. *J. Geophys. Res.,* **93,** 11 015–11 021.

Houghton, R., 1996: Subsurface quasi-decadal fluctuations in the North Atlantic. *J. Climate,* **9,** 1363–1373.

Hurrell, J. W., 1995: Decadal trends in the North Atlantic oscillation: Regional temperatures and precipitation. *Science,* **269,** 676–679.

Kalnay, E., and Coauthors, 1996: The NCEP/NCAR 40-Year Reanalysis Project. *Bull. Amer. Meteor. Soc.,* **77,** 437–471.

Koltermann, K. P., A. V. Sokov, V. P. Tereschenkov, S. A. Dobrliubov, K. Lorbacher, and A. Sy, 1999: Decadal changes in the thermohaline circulation of the North Atlantic. *Deep-Sea Res. II,* **46,** 109–138.

Kraus, E., and J. Turner, 1967: A one-dimensional model of the seasonal thermocline ii, the general theory and its consequences. *Tellus,* **19,** 98–105.

Kushnir, Y., 1994: Interdecadal variations in North Atlantic surface temperature and associated atmospheric conditions. *J. Climate,* **7,** 141–157.

Latif, M., K. Arpe, and E. Röckner, 2000: Oceanic control of decadal North Atlantic sea level pressure variability in winter, *Geophys. Res. Lett.,* **27,** 727–730.

Levitus, S., and T. P. Boyer, 1994: *Temperature.* Vol. 4, *World Ocean Atlas 1994,* NOAA Atlas NESDIS, 117 pp.

——, J. Antonov, and T. Boyer, 1994: Interannual variability of temperature at a depth of 125 meters in the North Atlantic Ocean. *Science,* **266,** 96–98.

Lorbacher, K., 2000: Niederfrequente Variabilitaet meridionaler Transporte in der Divergenzzone des Nordatlantischen Subtropen und Subpolarwirbels—der WOCE-Schnitt A2. Berichte des BSH Tech. Rep. 22, 156 pp.

MacDonald, A., and C. Wunsch, 1996: An estimate of global ocean circulation and heat fluxes. *Nature,* **382,** 436–439.

Mehta, V., M. Suarez, J. Manganello, and T. Delworth, 2000: Oceanic influence on the North Atlantic oscillation and associated Northern Hemisphere climate variations: 1959–1993. *Geophys. Res. Lett.,* **27,** 121–124.

Molinari, L., D. Mayer, J. Festa, and H. Bezdek, 1997: Multiyear variability in the near-surface temperature structure of the midlatitude western North Atlantic Ocean. *J. Geophys. Res.,* **102,** 3267–3278.

Pacanowski, R., 1995: MOM 2 documentation, user's guide and reference manual. GFDL Tech. Rep. 3, 123 pp.

Palmer, T., 1996: Predictability of the atmosphere and oceans: From days to decades. *Decadal Climate Variability,* D. Anderson and J. Willebrand, Eds., Springer-Verlag, 83–156.

Reverdin, G., D. Cayan, and Y. Kushnir, 1997: Decadal variability of hydrography in the upper northern North Atlantic 1948–1990. *J. Geophys. Res.,* **102,** 8505–8532.

——, N. Verbrugge, and H. Valdimarson, 1999: Upper ocean variability between Iceland and Newfoundland 1993–1998. *J. Geophys. Res.,* **104,** 29 599–29 611.

Rodwell, M., D. Rowell, and C. Folland, 1999: Oceanic forcing of the wintertime North Atlantic oscillation and European climate. *Nature,* **11,** 1906–1931.

Römmich, D., and C. Wunsch, 1985: Two transatlantic sections: Meridional circulation and heat flux in the subtropical North Atlantic. *Deep-Sea Res.,* **33,** 619–664.

Schott, F., T. Lee, and R. Zantopp, 1988: Variability of structure and transport of the Florida Current in the period range from days to seasonal. *J. Phys. Oceanogr.,* **18,** 1209–1230.

Smith, T., R. Reynolds, R. Livezey, and D. Stokes, 1996: Reconstruction of historical sea surface temperatures using empirical orthogonal functions. *J. Climate,* **9,** 1403–1420.

Stevens, D., 1990: On open boundary conditions for three dimensional primitive equation ocean circulation models. *Geophys. Astrophys. Fluid Dyn.,* **51,** 103–133.

Storch, H., T. Bruns, I. Fischer-Bruns, and K. Hasselmann, 1988: Principal Oscillation Pattern analysis of the 30- to 60-day oscillation in a general circulation model equatorial troposphere. *J. Geophys. Res.,* **93,** 11 022–11 036.

Wallace, J., and D. Gutzler, 1981: Teleconnections in the geopotential height field during the Northern Hemisphere winter. *Mon. Wea. Rev.,* **109,** 784–812.

Willebrand, J., S. Philander, and R. Pacanowski, 1980: The oceanic response to large-scale atmospheric disturbances. *J. Phys. Oceanogr.,* **10,** 411–429.